Receiver Design and On-Sun Testing for G3P3-USA

Clifford K. Ho,[1, a)] Nathaniel R. Schroeder,[1] Hendrik F. Laubscher, Lindsey Yue,[1] Brantley Mills,[2] Reid Shaeffer,[2] Joshua M. Christian,[1] and Kevin J. Albrecht[1]

[1]*Concentrating Solar Technologies, Sandia National Laboratories, P.O. Box 5800, MS-1127, Albuquerque, NM 87185-1127, USA*
[2]*Thermal Sciences & Engineering, Sandia National Laboratories, P.O. Box 5800, Albuquerque, NM 87185, USA*

[a)]Corresponding author: ckho@sandia.gov

Abstract. This paper summarizes the evolution of the Gen 3 Particle Pilot Plant (G3P3) receiver design with the goal of reducing heat losses and increasing thermal efficiencies. New features that were investigated included aperture covers and shrouds, active airflow, multistage catch-and-release devices (stairs), and optimization of receiver cavity geometry. Simulations and ground-based testing showed that a reduced receiver volume and aperture shroud could reduce advective heat losses by ~40 – 50%, and stairs could increase opacity and reduce backwall temperatures. The reduced volume receiver and stairs were selected for on-sun testing, and receiver efficiencies up to 80 – 90% were achieved in the current test campaign. The receiver thermal efficiency generally increased as a function of incident power and particle mass flow rates. In addition, particle outlet temperatures were maintained to within ±10 °C of a prescribed setpoint temperature up to ~700 °C using a PID controller that adjusted the particle mass flow rate into the receiver in response to the measured particle outlet temperatures.

INTRODUCTION

Sandia National Laboratories is leading an effort to design a next-generation particle-based concentrating solar power (CSP) plant as part of the Gen 3 Particle Pilot Plant (G3P3) project sponsored by the U.S. Department of Energy's Solar Energy Technologies Office. The goal of G3P3-USA* is to design, construct, and operate a pilot-scale system that heats particles from ~600 °C to ~775 °C in a > 1 MW_t falling particle receiver (FPR) with 6 MWh of thermal storage [1] (**FIGURE 1**). The hot particles are passed through a particle-to-working-fluid heat exchanger to heat supercritical CO_2 from ~565 °C to ~715 °C at ~20 - 25 MPa. The goal of the first two years of the project, which began in 2018, was to de-risk particle-based technologies through modeling and testing of the key components: particle receiver, storage, heat exchanger, and lift.

One of the key risks is the receiver thermal efficiency, defined as the power absorbed by the irradiated particles falling through the receiver divided by the incident power entering the receiver aperture. Previous studies have shown that advective heat losses induced by particle entrainment and wind can significantly reduce the receiver efficiency [2, 3]. This paper describes the evolution of receiver designs considered in G3P3-USA and the key on-sun tests that will be performed in the summer of 2020 to demonstrate new design features intended to mitigate heat losses and increase receiver efficiencies.

* A parallel effort is being performed by King Saud University to develop a G3P3-KSA system using air as the working fluid in a Brayton cycle. The G3P3-KSA system employs obstructions to slow the particle flow.

EVOLUTION OF G3P3 RECEIVER DESIGNS

FIGURE 2 shows the evolution of various design considerations since the start of the G3P3-USA project. The initial design that was previously tested at Sandia from 2015 - 2016 is shown on the left, which yielded on-sun receiver efficiencies of ~60 – 80% [4]. Additional features were simulated and/or tested during the G3P3 project to reduce heat losses (primarily advective), which included aperture covers and shrouds, active airflow, multistage catch-and-release devices, and optimization of receiver cavity geometry. Based on the results of these studies, designs were downselected for on-sun testing. The following provides an overview of the designs and findings:

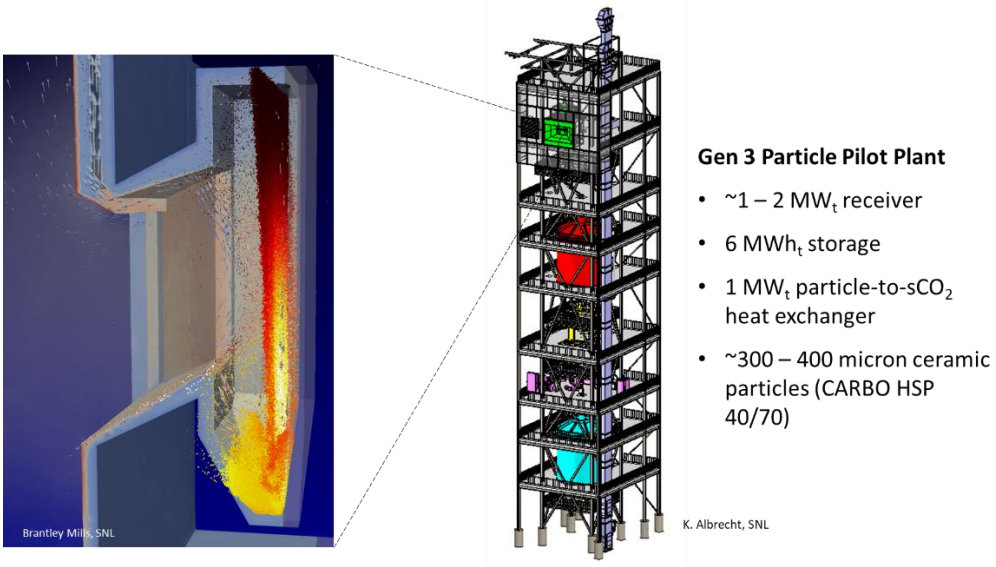

FIGURE 1. Drawing of the proposed G3P3-USA system and an expanded view of particle flow and heating in the receiver.

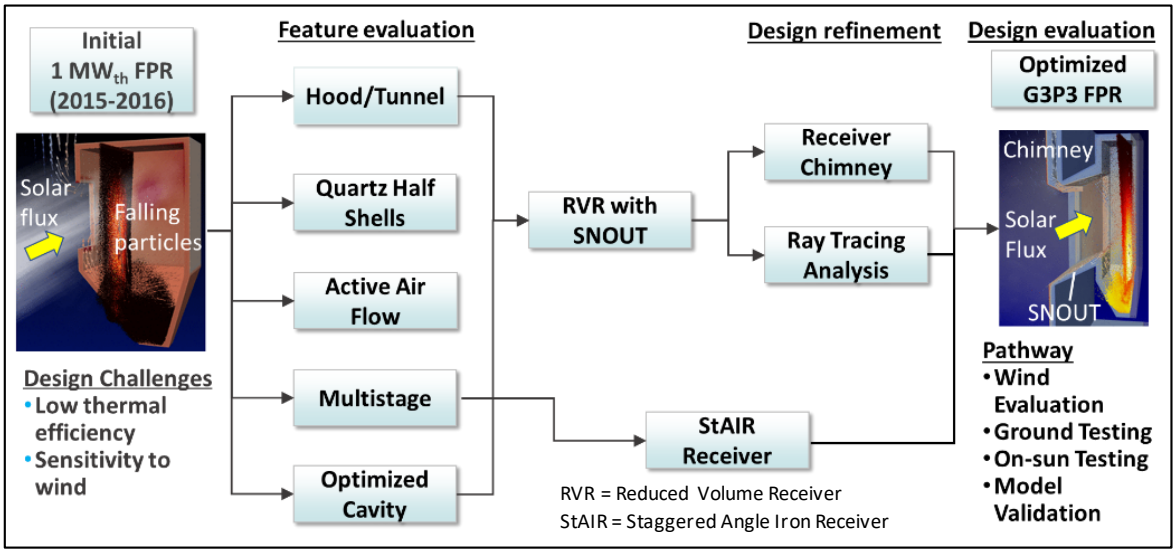

FIGURE 2. Evolution of G3P3 falling particle receiver (FPR) design and testing.

Aperture Covers: Simulations of quartz half-shell tubes covering the receiver aperture did not show significant improvement due to a "short-circuiting" effect of thermal radiation from the hot quartz shells to the external environment [5, 6]. In addition, quartz aperture covers were not scalable to commercial sizes (tens of meters). Therefore, the use of quartz half-shell aperture covers was not pursued or considered for on-sun testing.

Aperture Shrouds: Aperture hoods and shrouds (SNOUT – Sandia Nod Optimized Unobstructed Tunnel) were simulated, and results showed up to ~20% reduction in advective heat losses [2, 7]. A chimney in the SNOUT was also designed to capture particle fines. Off-sun SNOUT tests were performed and showed a reduction in heat losses, but on-sun tests of the SNOUT were not planned in 2020 due to resource limitations.

Geometry Optimization: Receiver optimization studies resulted in a reduced volume receiver (RVR) that minimized the gap between the particle curtain and back wall, which reduced cold-air entrainment and advective heat losses [8]. An RVR configuration was included for on-sun testing in the summer of 2020.

Active Airflow: Simulations of active airflow devices (air curtains across the aperture and air withdrawal at various points within the receiver to prevent advective heat loss) showed that these devices were not reliable in the presence of wind [9]. Therefore, active airflow will not be pursued in the on-sun tests or G3P3 design.

Multistage release: Simulations and unheated particle flow testing of catch-and-release devices (StAIR – Staggered Angle Iron Receiver) were performed to increase the particle curtain opacity and prevent spreading due to gravitational acceleration of the falling particles were performed [10, 11]. Results showed that both the opacity and receiver efficiency could be increased with optimal spacing and design of the catch-and-release devices. Prototypes are being constructed for the on-sun tests in 2020.

ON-SUN TESTING

Based on the results of the simulations and tests described above, on-sun receiver tests were performed in 2020 at the National Solar Thermal Solar Test Facility (NSTTF) at Sandia National Laboratories to evaluate features and designs that showed promise in reducing receiver heat losses for the G3P3 system. In addition, a method to control particle outlet temperatures using a proportional-integral-derivative (PID) controller implemented in the data acquisition and control system was tested. The PID was used to control a slide gate to automatically adjust particle mass flow rates entering the receiver based on the particle outlet temperatures. If the particle outlet temperature exceeded the desired setpoint, the PID would adjust the slide gate to increase the particle mass flow into the receiver to reduce the particle temperatures, and vice-versa. In addition, 3-D ultrasonic wind anemometers were installed around the receiver to collect transient wind data to better understand transient wind impacts on particle receiver performance. Instrumentation, data acquisition, and protocols used during on-sun testing of the falling particle receiver have been documented in previous publications [1, 12-16]. **TABLE 1** summarizes the high-level goals of the 2020 test campaign.

TABLE 1. Summary of goals of on-sun receiver tests in 2020.

Feature	Conditions	Goal
Reduced volume receiver (RVR)	Up to 700 °C particle temperature; 500 – 1000 kW/m^2; 5 – 10 kg/s particle flow	Measure impact of reduced receiver-cavity volume on thermal efficiency; validate model
Multistage release	Up to 700 °C particle temperature; 500 – 1000 kW/m^2; 5 – 10 kg/s particle flow	Measure impact of catch-and-release devices on backwall temperatures and thermal efficiency; validate model
Temperature control	Perturb irradiance by up to 50% by adjusting number of heliostats and recording change in incident power level	Use closed-loop feedback to maintain particle temperatures within ±10°C of setpoint temperature using slide-gate-controlled particle mass flow
Additional wind characterization	Use five additional ultrasonic wind anemometers around the receiver	Collect wind data to understand wind perturbations and impact on receiver efficiency

Multi-Stage Release

Yue et al. [10] and Shaeffer et al. [11] investigated different designs and orientations for multi-stage particle catch-and release devices using the StAIR concept (**FIGURE 3**). The goal is to increase the particle-curtain opacity, increase flow stability, reduce backwall temperatures, and increase thermal efficiency. By cascading the particles forward over the structures, the particles protect the stairs from direct irradiance and overheating. Simulations showed that the thermal efficiency would not be increased substantially for the small-scale system (up to several percent [11], which

is within the uncertainty range of measurements during on-sun tests). However, the simulated opacity increased, yielding a significant decrease in backwall temperatures. Based on these tests and simulations, stairs of a prescribed shape and orientation were placed in the particle receiver for on-sun testing (**FIGURE 4**).

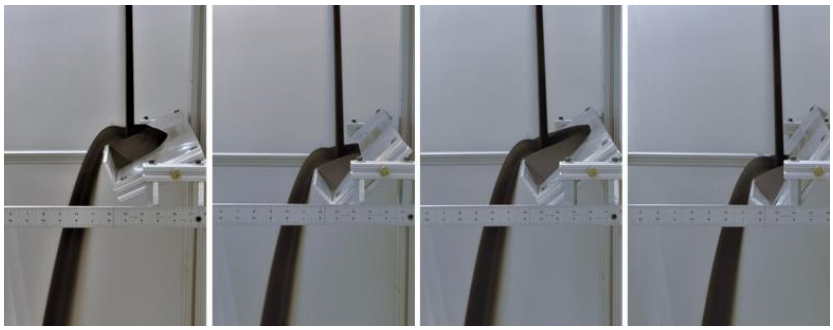

FIGURE 3. Testing to evaluate particle flow over different StAIR designs and orientations [10].

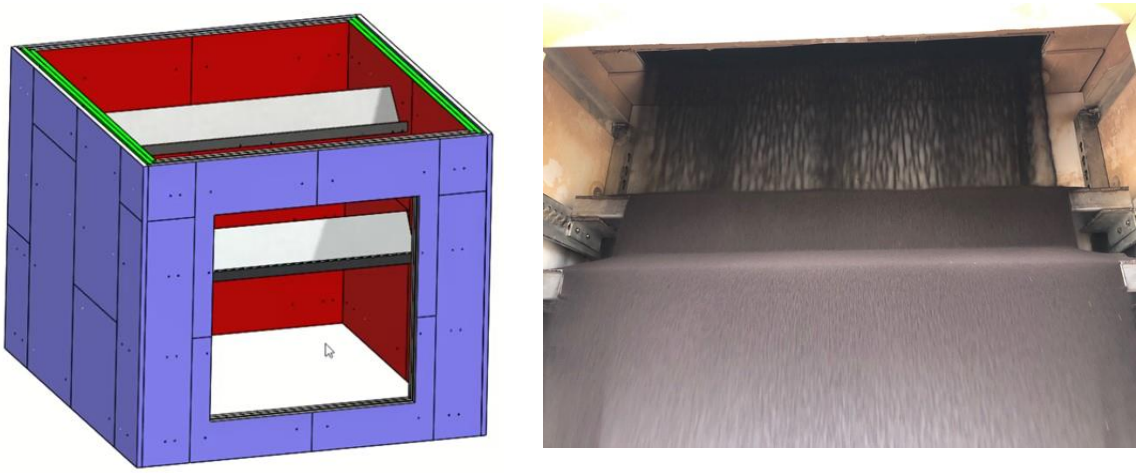

FIGURE 4. Left: drawing of two stairs in receiver. Right: Particle flow over two stairs in receiver showing improvement in particle flow and opacity relative to free-fall particle flow and opacity above the stairs.

Reduced Volume Receiver

Optimization of the G3P3 receiver was performed using computational fluid dynamics (CFD) simulations and probabilistic modeling [8]. Results showed that a reduced receiver volume that was narrower could prevent advective recirculation and heat loss behind the particle curtain. With the reduced volume receiver geometry, simulated airflow entrained by the particles was redirected to impede cold ambient air entering the aperture.

Ground-based testing using electrically heated particles to ~500 °C was performed with and without a partition to evaluate the impacts of a reduced volume. Both experiments and simulations of the reduced volume resulted in nearly a 40% reduction in advective heat loss. **FIGURE 5** shows a schematic of the particle receiver before and after insertion of the partition, which was made of Zircar RSLE-57 refractory board [17]. RSLE-57 is the same material used for the walls of the receiver and the heatshield around the aperture. As shown in **FIGURE 5** (left), the original design allowed cold ambient air to be pulled into the receiver while hot air recirculated behind the curtain. Inclusion of the partition reduced advection behind particle curtain, forcing entrained air from the falling particles to circulate in front of the aperture, impeding some of the incoming ambient air.

Because the ground-based tests (without irradiance) used the partition as the last set of tests before lifting the receiver assembly to the top of the tower, the on-sun tests began with the partition in place. As of the date of this paper, tests were still being performed with the reduced volume, and plans are to remove the partition for comparison to the baseline test after all on-sun tests with the reduced volume and stairs have been completed.

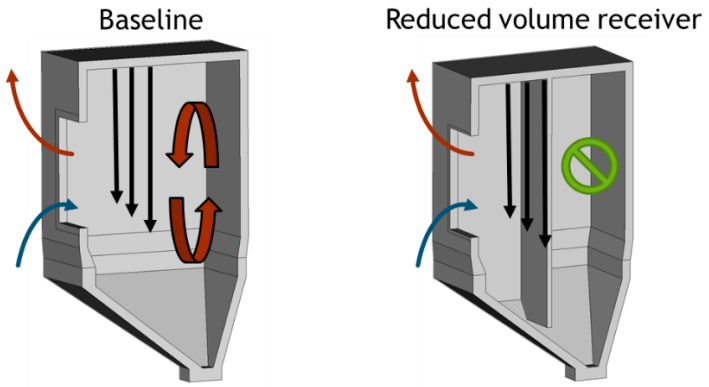

FIGURE 5. Left: Original receiver design showing cold ambient air being pulled into the receiver and hot air recirculated behind the curtain. Right: Insertion of partition to reduce cavity volume and advection behind particle curtain, forcing entrained air to circulate in front of the aperture, impeding some of the incoming ambient air.

Results

TABLE 2 summarizes the on-sun receiver tests performed in August and September of 2020, including the calculated thermal efficiency. The receiver thermal efficiency, η_{th}, was calculated as the ratio of the net particle-absorbed power, $Q_{abs,net}$ (W), and the total incident power, Q_{in}, entering the receiver aperture:

$$\eta_{th} = \frac{Q_{abs,net}}{Q_{in}} = \frac{\dot{m}\left(h_{out} - h_{in}\right)}{Q_{in}} = \frac{\dot{m}\int_{T_{in}}^{T_{out}} c_p\left(T\right)dT}{Q_{in}} = \frac{\dot{m}\left[113.2\left(T_{out}^{1.3093} - T_{in}^{1.3093}\right)\right]}{Q_{in}} \quad (1)$$

where h_{in} and h_{out} are the particle enthalpy (J/kg) at the receiver inlet and outlet, respectively, and T_{in} and T_{out} are the measured average particle temperatures (K) at the receiver inlet and outlet, respectively. The particle inlet temperature is measured by thermocouples, which are immersed in the particles, above the exit of the top hopper. The particle outlet temperatures are measured by thermocouples at the base of five equally spaces funnels near the outlet of the receiver that ensure the thermocouples are immersed in the particles. The solar irradiance distribution and total incident power were measured using a combination of a Kendall radiometer placed in the middle of a water-cooled flux target and a camera-based beam characterization system (BCS) [15, 16, 18, 19]. Prescribed heliostats were aimed toward the flux target prior to being aimed at the receiver aperture. The Kendall radiometer was used to measure the irradiance at a single point, which was used to scale each pixel value within the corresponding area of the receiver aperture recorded by the BCS to determine the incident power [18]. This method was compared to the PHLUX method [20] and was shown to yield total incident power values that were generally within a few percent. Measurement errors for each of the measured quantities in were propagated to the final efficiency calculation in Eq. (1). The specific heat of CARBO HSP 40/70 (nominal particles size ~400 – 500 microns) was measured at Sandia using a Netzsch STA 409 CD DSC with argon atmosphere from room temperature to ~1000 °C. The resulting expression for the specific heat, c_p (J/kg-K), is as follows with an R^2 of 0.9732:

$$c_p = 148.2T(K)^{0.3093} \quad (2)$$

The on-sun tests shown in **TABLE 2** explored different irradiance values, mass flow rates, stair configurations, temperatures, and environmental conditions (ambient temperature, wind speed and direction). The goal is to record as many tests as possible under a variety of conditions to develop a better understanding and appropriate correlations for the receiver efficiency as a function of the independent parameters. In particular, previous simulations have shown a significant impact of wind direction on receiver efficiency, but a lack of test data with recorded wind speeds and direction around the receiver assembly made it difficult to validate the models [2]. The current test campaign is still in process, but we intend to use the data from the five 3-D ultrasonic wind anemometers to better characterize the test conditions for model validation.

TABLE 2. Summary of on-sun tests conducted through September 25, 2020 (average values shown).

Date	Peak Irradiance (kW/m^2)	Mass Flow Rate (kg/s)	Tin (°C)	Tout (°C)	Thermal Efficiency	Ambient T (°C)	Wind Speed (m/s)	Wind Direction[1]	Number of Stairs
8/17/2020	680	2.38	545	629	42%	31	3.2	251	2
8/17/2020	1150	8.09	534	611	75%	31	4.4	159	2
8/18/2020	590	6.43	667	715	78%	28	2.8	170	2
8/18/2020	1200	6.47	584	692	83%	30	1.8	325	2
8/20/2020	430	2.96	307	391	63%	30	1.0	304	2
8/20/2020	410	5.90	534	578	73%	32	1.8	219	2
8/20/2020	440	5.81	661	704	76%	32	0.9	304	2
8/20/2020	450	5.77	606	654	82%	33	2.6	288	2
8/21/2020	450	5.79	585	630	78%	28	5.2	348	1
8/21/2020	330	7.48	323	356	80%	29	1.8	273	1
8/21/2020	410	5.79	581	630	91%	30	2.9	331	1
9/4/2020	490	6.46	680	716	65%	27	2.1	214	1
9/4/2020	600	6.69	528	575	66%	28	3.7	239	1
9/4/2020	560	9.19	546	570	76%	28	1.9	282	1
9/4/2020	600	6.40	627	682	79%	29	1.9	237	1
9/18/2020	630	9.27	573	595	43%	21	2.9	242	1
9/18/2020	690	9.02	779	802	45%	22	2.9	296	1
9/18/2020	600	7.61	585	613	48%	22	3.3	221	1
9/18/2020	690	10.07	776	799	49%	22	2.7	261	1
9/18/2020	680	8.24	752	788	64%	23	3.9	256	1
9/18/2020	680	7.19	692	735	71%	23	1.3	272	1
9/18/2020	560	4.23	512	586	74%	23	2.2	204	1
9/18/2020	550	5.29	484	551	83%	23	2.5	237	1
9/22/2020	80	7.35	438	442	50%	26	3.3	291	1
9/22/2020	160	7.35	428	440	64%	26	1.4	312	1
9/22/2020	240	7.35	413	431	64%	26	4.1	345	1
9/22/2020	310	7.35	410	438	76%	26	4.2	285	1
9/22/2020	420	7.35	432	469	76%	26	5.0	287	1
9/22/2020	530	7.01	446	497	82%	26	4.0	303	1
9/22/2020	680	7.25	435	502	86%	27	4.3	292	1
9/24/2020	90	3.89	490	490	47%	27	3.3	287	1
9/24/2020	350	4.57	457	457	55%	27	3.3	329	1
9/24/2020	180	3.88	477	477	55%	27	2.9	290	1
9/24/2020	270	3.88	465	504	64%	27	5.4	303	1
9/24/2020	500	4.30	489	489	73%	27	3.4	281	1
9/24/2020	600	4.67	482	482	75%	27	5.7	285	1
9/24/2020	470	4.67	459	459	76%	27	2.8	293	1
9/24/2020	680	4.67	511	511	84%	27	4.4	277	1
9/24/2020	660	4.67	511	511	87%	27	4.4	275	1
9/25/2020	90	7.46	478	481	23%	28	4.7	330	1
9/25/2020	180	7.90	466	477	58%	28	3.9	311	1
9/25/2020	480	7.39	473	505	61%	28	5.7	303	1
9/25/2020	360	7.39	473	499	65%	28	5.5	296	1
9/25/2020	270	7.90	460	478	65%	28	4.4	321	1
9/25/2020	710	6.85	548	607	74%	28	7.8	303	1
9/25/2020	710	7.31	515	576	80%	28	5.9	287	1
9/25/2020	620	7.39	479	534	83%	28	3.4	320	1

[1]Wind direction: 0° = north wind (from the north), 90° = east wind, 180° = south wind

FIGURE 6 shows a sample temperature profile of the particle temperatures entering and exiting the receiver during an on-sun test on Aug. 20, 2020. The irradiance values for this particular test day were relatively low (340 – 400 kW/m^2), but the particle temperatures increased to over 700 °C. During the course of the tests, the heliostats were occasionally moved from the receiver to the adjacent water-cooled calibration panel to measure the irradiance and power using a beam characterization system. In addition, the flow from the particle screw elevator was periodically stopped to measure the mass flow entering the receiver using load cells at the base of the top hopper. These measurements caused periodic perturbations in the measured particle outlet temperatures. In addition, periods of particle recirculation and cooling (without solar irradiance) were applied to allow the particles to cool before applying new irradiance values or particle mass flow rates.

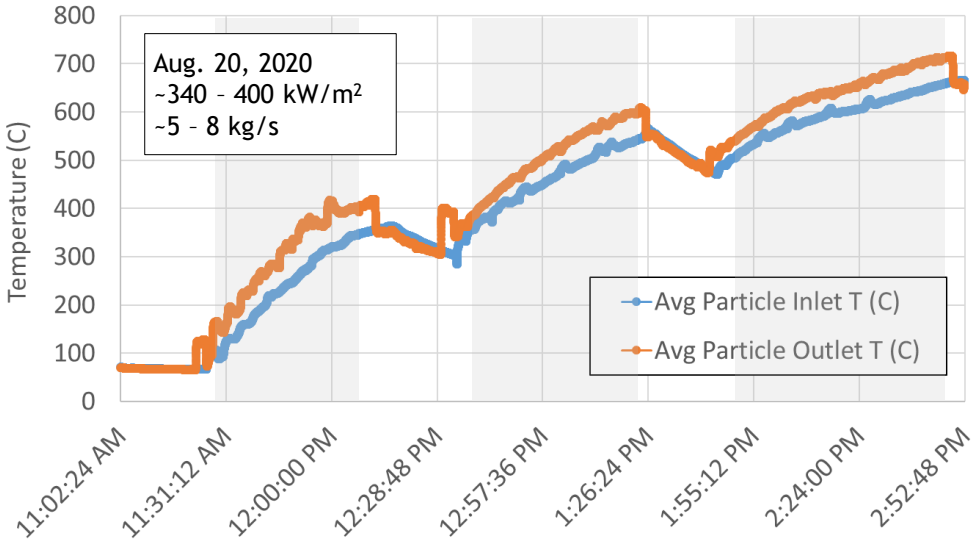

FIGURE 6. Sample temperature profile during on-sun testing.

The temperatures in the shaded regions in **FIGURE 6** were used to calculate the thermal efficiency using Eq. (1). Measurement errors and uncertainties were propagated [12], and the resulting average and uncertainties in the calculated receiver thermal efficiency are shown in **FIGURE 7**. Both current results (using either one or two stairs) and freefall results from Ho et al. 2019 [19] are shown. In addition, the theoretical maximum receiver thermal efficiency, $\eta_{th,max}$, is plotted for reference and is calculated as follows:

$$\eta_{th,\max} = \frac{\alpha Q_{in} - Q_{loss}}{Q_{in}} = \alpha - \frac{\varepsilon\sigma A\left(T_{p,ave}^4 - T_{amb}^4\right) + hA(T_{p,ave} - T_{amb})}{Q_{in}} = 1 - \frac{\sigma A\left(T_{p,ave}^4 - T_{amb}^4\right)}{Q_{in}} \quad (3)$$

where α is the effective absorptance of the particles in the cavity receiver (=1 for theoretical maximum), Q_{in} is the incident power entering the aperture (W), Q_{loss} is the total (radiative and convective) heat loss (W) through the aperture, ε is the radiative thermal emissivity (assumed to be 1 for a cavity receiver), σ is the Stefan-Boltzmann constant (5.67×10^{-8} W/m^2-K^4), A is the receiver aperture area (1 m^2), $T_{p,ave}$ is the average particle temperature (K), T_{amb} is the ambient temperature (K), and h is the falling particle convective heat transfer coefficient (=0 for theoretical maximum). It is important to note that Eq. (3) is not intended to predict the thermal efficiencies of the current tests. It is only provided to serve as a theoretical maximum in **FIGURE 7** and **FIGURE 8** to illustrate how higher theoretical efficiencies can be obtained at higher incident powers but with an asymptotic trend. Detailed CFD modeling has been performed with previous tests to provide detailed physics-based predictions and comparisons to the measured particle temperature rise and thermal efficiencies [3, 21]. CFD modeling is currently being performed for the current set of on-sun tests and will be presented in a future paper.

For the purposes of illustrating the theoretical maximum efficiency, an average particle temperature is assumed to be 650 °C (923 K) in Eq. (3), and the resulting theoretical maximum efficiency is plotted in **FIGURE 7** as a solid black line; note that tests with lower particle temperatures may yield receiver efficiencies that exceed the theoretical

maximum efficiency at 650 °C. Results show that the both the theoretical and measured receiver efficiencies tend to increase with increasing incident power since the fraction of heat losses to input power is less (see Eq. (3)). Measured receiver efficiencies that are less than ~60% tend to be a result of low irradiance, low particle mass flow (which allows for more transmittance through the particle curtain), high temperatures, or some combination of these factors. In addition, wind can also lower the receiver efficiency, especially if the wind originates from a direction within ~90° from the aperture normal [2].

FIGURE 8 shows a subset of the test results to better elucidate some of the effects of mass flow, irradiance, and the potential impact of the stairs. All of the tests were run at particle inlet temperatures between 400 – 500 °C, and results with a single stair show that the receiver efficiency tends to increase with increasing particle mass flow rate. Results from freefall tests conducted in 2018 [19] that are included in the test were performed at higher irradiances than the tests with the stair, but extrapolation of the single-stair results at similar mass flow rates (7 – 9 kg/s) to higher irradiances appears to yield efficiencies that will surpass the freefall results. Due to persistent smoke and haze from surrounding wildfires in California and Colorado during the current test campaign, there was more scatter in the beam that caused overheating and damage of the frame around the aperture. Therefore, the peak flux was generally kept below 600 kW/m^2 peak for most of the current tests. Future tests will attempt to reach higher irradiances (~1000 kW/m^2) when the smoke and haze clear. In addition, future tests will remove the partition to compare the results of the reduced volume receiver with the original baseline configuration.

FIGURE 9 shows a test where the particle outlet temperature was maintained by the PID controller using different setpoint temperatures. The power entering the aperture was maintained at ~300 – 500 kW (peak irradiance ~400 – 600 kW/m^2) except when heliostats were moved briefly to the adjacent calibration panel to measure the irradiance and power, which caused sudden decreases in the particle inlet temperature. Because the system does not have active particle cooling, the particle inlet temperatures continue to increase during normal operation as the irradiated particles heat up and circulate through the system. The slide gate can move to any desired opening in less than one second, and the time required to reach a desired particle setpoint temperature was shown to be less than one minute in past studies [12], which used a simple proportional control algorithm. The implementation of a full PID in this study reduced some of the oscillations observed in previous studies when large flux perturbations were induced, but the dampening effect of the PID controls increased the response time to reach the setpoint temperature in some cases. Additional tuning of the PID parameters will be continued in future testing.

FIGURE 9 shows that as particle inlet temperatures increase, the particle outlet temperature is maintained at the prescribed setpoint temperature by the PID controller, which increases the particle mass flow rate to reduce the increase in temperature for a fixed incident power. The setpoint had to be increased periodically when the slide gate could not increase any further to reduce the particle outlet temperature. The PID controller generally maintained the particle outlet temperature to ±10 °C of the setpoint temperature, which was the desired tolerance. However, when the setpoint of the particle outlet temperature reached 750 °C, the controller was not able to maintain the temperature reliably. We postulate that higher irradiances and incident power may be required to more reliably control the particle outlet temperatures at or above ~750 °C. Future tests will employ additional power (when the smoke and haze clear), and prescribed perturbations of the heliostat field will be applied to simulate impacts of periodic cloud cover. Optimization of the PID parameter values will also be investigated.

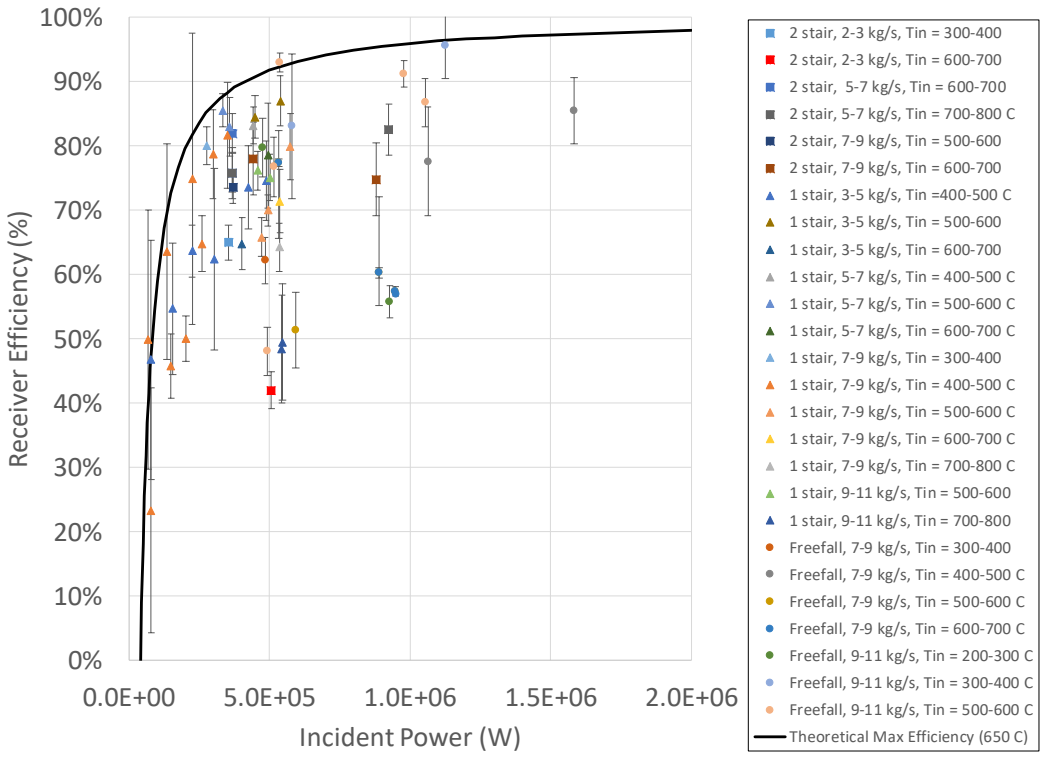

FIGURE 7. Plot of receiver efficiencies for on-sun StAIR tests (including freefall tests from 2018 [19]) and theoretical maximum efficiency (solid black line) at 650 °C (note: tests conducted at lower temperatures could yield higher efficiencies than theoretical maximum).

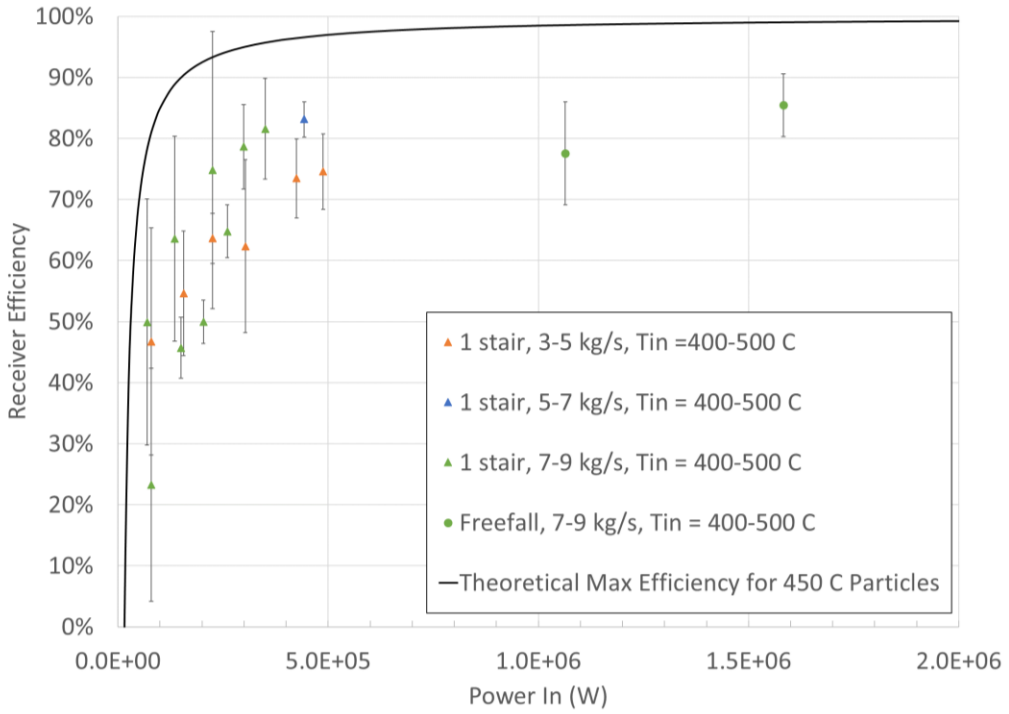

FIGURE 8. Plot of receiver efficiencies for on-sun StAIR tests (including freefall tests from 2018 [19]) with particle inlet temperatures between 400 – 500 °C and theoretical maximum efficiency (solid black line) at 450 °C.

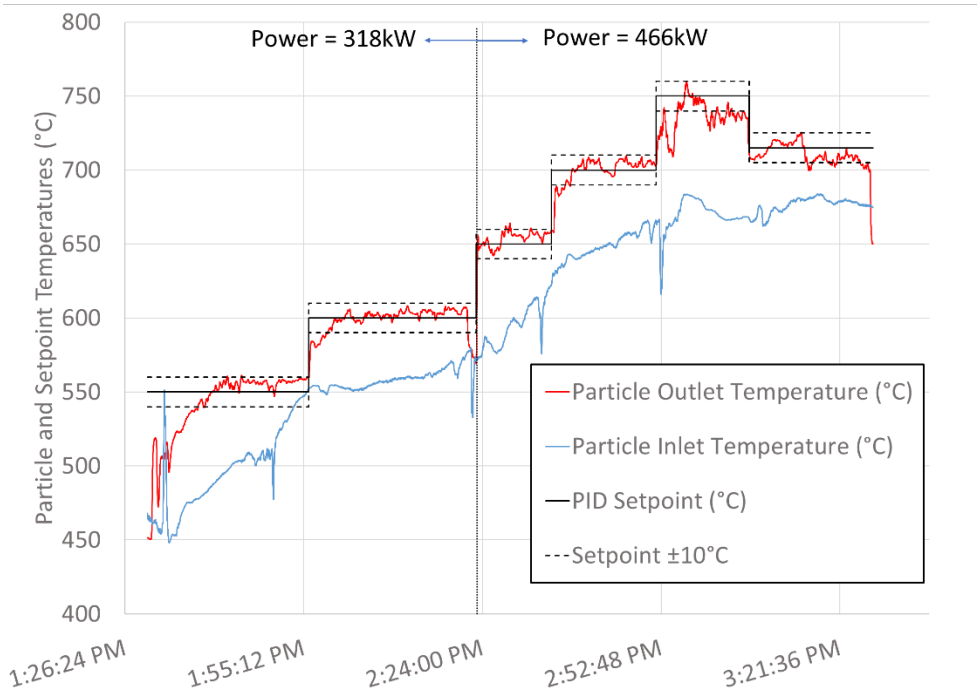

FIGURE 9. Particle temperature control test on Oct. 8, 2020.

CONCLUSIONS

This paper summarized the evolution of the G3P3 receiver design, which included investigation of aperture covers, shrouds, active airflow, geometry optimization, and multistage catch-and-release structures to increase the receiver thermal efficiency. Based on the results of simulations and experiments, a reduced receiver volume concept and catch-and-release stairs were implemented for on-sun testing. Results of the tests showed that the receiver thermal efficiency generally increased with increasing incident power and particle mass flow rate. The impact of the StAIRs and the reduced volume have not been rigorously quantified, but extrapolations comparing the results of recent StAIR tests with previous freefall tests indicate that the StAIR configuration appears to yield improved efficiencies. Tests were also performed using a PID controller to maintain the particle outlet temperatures to prescribed setpoint temperatures. Results showed that the PID controller could maintain particle outlet temperatures to within ±10 °C of the prescribed setpoint up to temperatures of ~700 °C. Future tests will evaluate higher incident power and irradiance levels when the smoke and haze from surrounding wildfires clear, and the partition for the reduced volume receiver tests will be removed. Simulations of these on-sun tests will also be performed for model validation with inclusion of additional wind characterization.

ACKNOWLEDGMENTS

The authors thank Daniel Ray, Luis Garcia Maldonado, Lonnie Haden, Kevin Good, Lam Banh, Roger Buck, Benson Tso, Robert Crandell, Francisco Alvarez, Nicolas Delovato, and Rip Winckel for their assistance with the on-sun testing.

This work is funded in part or whole by the U.S. Department of Energy Solar Energy Technologies Office under Award Number 34211. This report was prepared as an account of work sponsored by an agency of the United States Government. Neither the United States Government nor any agency thereof, nor any of their employees, makes any warranty, express or implied, or assumes any legal liability or responsibility for the accuracy, completeness, or usefulness of any information, apparatus, product, or process disclosed, or represents that its use would not infringe privately owned rights. Reference herein to any specific commercial product, process, or service by trade name, trademark, manufacturer, or otherwise does not necessarily constitute or imply its endorsement, recommendation, or favoring by the United States Government or any agency thereof. The views and opinions of authors expressed herein do not necessarily state or reflect those of the United States Government or any agency thereof.

Sandia National Laboratories is a multimission laboratory managed and operated by National Technology and Engineering Solutions of Sandia, LLC., a wholly owned subsidiary of Honeywell International, Inc., for the U.S. Department of Energy's National Nuclear Security Administration under contract DE-NA0003525.

REFERENCES

1. C. K. Ho, K. J. Albrecht, L. Yue, B. Mils, J. Sment, J. Christian and M. Carlson, *Overview and Design Basis for the Gen 3 Particle Pilot Plant (G3P3)*, in *SolarPACES 2019*, Daegu, South Korea,
2. B. Mills, R. Shaeffer, C. K. Ho and L. Yue, *Modeling the Thermal Performance of Falling Particle Receivers Subject to External Wind*, in *Proceedings of the ASME 2019 13th International Conference on Energy Sustainability*, ES2019-3913, Bellevue, WA, July 15 - 18, 2019.
3. B. Mills and C. K. Ho, *Simulation and Performance Evaluation of On-sun Particle Receiver Tests*, in *SolarPACES 2018*, Cassablanca, Morocco,
4. C. K. Ho, J. M. Christian, J. Yellowhair, S. Jeter, M. Golob, C. Nguyen, K. Repole, S. I. Abdel-Khalik, N. Siegel, H. Al-Ansary, A. El-Leathy and B. Gobereit, *Highlights of the High-Temperature Falling Particle Receiver Project: 2012 - 2016*, in *SolarPaces 2016: International Conference on Concentrating Solar Power and Chemical Energy Systems*, Abu Dhabi, UAE, October 11 - 14, 2016.
5. J. Yellowhair and C. K. Ho, *Optical Ray-Tracing Performance Modeling Of Quartz Half-Shell Tubes Aperture Cover For Falling Particle Receiver*, in *Proceedings of the ASME 2019 13th International Conference on Energy Sustainability*, ES2019-3927, Bellevue, WA, July 15 - 18, 2019.
6. L. Yue, B. Mills and C. K. Ho, *Effect of Quartz Aperture Covers on the Fluid Dynamics and Thermal Efficiency of Falling Particle Receivers*, in *Proceedings of the ASME 2019 13th International Conference on Energy Sustainability*, ES2019-3910, Bellevue, WA, July 15 - 18, 2019.

7. B. Mills, R. Shaeffer, L. Yue and C. K. Ho, *Improving Next-generation Falling Particle Receiver Designs Subject to Anticipated Operating Conditions*, in *ASME 2020 14th International Conference on Energy Sustainability*, Denver, CO, June 7 - 11, 2020.
8. B. Mills, B. Schroeder, L. Yue, R. Shaeffer and C. K. Ho, *Optimizing a Falling Particle Receiver Geometry Using CFD Simulations to Maximize the Thermal Efficiency*, in *SolarPACES 2019*, Daegu, South Korea, October 1 - 4, 2019.
9. L. Yue, R. Schaeffer, B. Mills and C. K. Ho, *Active Airflow for Reducing Advective and Particle Loss in Falling Particle Receivers*, in *SolarPACES 2019*, Daegu, South Korea, October 1 - 4, 2019.
10. L. Yue, N. Schroeder and C. K. Ho, *Particle Flow Testing of a Multistage Falling Particle Receiver Concept: Staggered Angle Iron Receiver (StAIR)*, in *ASME 2020 14th International Conference on Energy Sustainability*, Virtual Online, June 17 - 18, 2020.
11. R. Shaeffer, B. Mills, L. Yue and C. K. Ho, *Evaluation of Performance Factors for a Multistage Falling Particle Receiver*, in *ASME 2020 14th International Conference on Energy Sustainability*, Virtual Online Conference, June 17 - 18, 2020.
12. C. K. Ho, G. Peacock, B. Mills, J. M. Christian, K. Albrecht, J. E. Yellowhair and D. Ray, *Particle Mass Flow Control for High-Temperature Concentrating Solar Receivers*, 2018.
13. C. Ho, J. Christian, D. Gill, A. Moya, S. Jeter, S. Abdel-Khalik, D. Sadowski, N. Siegel, H. Al-Ansary, L. Amsbeck, B. Gobereit and R. Buck, *Technology advancements for next generation falling particle receivers*, Proceedings of the Solarpaces 2013 International Conference **49** (Energy Procedia), 398-407 (2014).
14. C. K. Ho, J. M. Christian, D. Romano, J. Yellowhair, N. Siegel, L. Savoldi and R. Zanino, *Characterization of Particle Flow in a Free-Falling Solar Particle Receiver*, J Sol Energ-T Asme **139** (2) (2017).
15. C. K. Ho, J. M. Christian, J. Yellowhair, N. Siegel, S. Jeter, M. Golob, S. I. Abdel-Khalik, C. Nguyen and H. Al-Ansary, *On-Sun Testing of an Advanced Falling Particle Receiver System*, Solarpaces 2015: International Conference on Concentrating Solar Power and Chemical Energy Systems **1734** (2016).
16. C. K. Ho, J. M. Christian, J. E. Yellowhair, K. Armijo, W. J. Kolb, S. Jeter, M. Golob and C. Nguyen, *On-Sun Performance Evaluation of Alternative High-Temperature Falling Particle Receiver Designs*, J Sol Energ-T Asme **141** (1) (2019).
17. I. ZIRCAR Refractory Composites. *High Temperature Refractory Composites and Related Products for use as Thermal, Electrical and Structural Insulation*. 2013 6/19/2013]; Available from: http://www.zrci.com/.
18. C. E. Andraka, J. M. Christian, C. M. Ghanbari, D. D. Gill, C. K. Ho, W. J. Kolb, T. A. Moss, E. J. Smith and J. Yellowhair, *Sandia Capabilities for the Measurement, Characterization, and Analysis of Heliostats for CSP*, Report No. SAND2013-5492, 2013.
19. C. K. Ho, G. Peacock, J. M. Christian, K. Albrecht, J. E. Yellowhair and D. Ray, *On-Sun Testing of a 1 MWt Particle Receiver with Automated Particle Mass-Flow and Temperature Control*, Solarpaces 2018: International Conference on Concentrating Solar Power and Chemical Energy Systems **2126** (2019).
20. C. K. Ho and S. S. Khalsa, *A Photographic Flux Mapping Method for Concentrating Solar Collectors and Receivers*, J Sol Energ-T Asme **134** (4) (2012).
21. C. K. Ho, S. S. Khalsa and N. P. Siegel, *Modeling on-Sun Tests of a Prototype Solid Particle Receiver for Concentrating Solar Power Processes and Storage*, in *ES2009: Proceedings of the ASME 3rd International Conference on Energy Sustainability, Vol 2*, San Francisco, CA,